NUMERICAL INVESTIGATIONS OF ADVANCED VOLUMETRIC RECEIVER MATERIALS

Olena Smirnova[1,2], Georg Bleiber[2], Christoph Jakob[2], Daniel Schöllgen[2], Thomas Fend[2] and Peter Schwarzbözl[2]

[1]Corresponding author: Tel. +492203 601 2901, olena.smirnova@dlr.de

[2]German Aerospace Center, Solar Research, Linder Hoehe, 51147 Koeln, Germany

Abstract

This paper presents the results of a numerical analysis of the mass transport and the heat flow through a volumetric solar receiver as a candidate component for a central receiver system for solar electricity generation. The receiver investigated was an extruded honeycomb structure made out of Silicon carbide. The objective of the study is to investigate the influence of slight geometric changes on to the overall performance of the receiver. The results are compared with those of an experimental study. Two numerical models have been developed. One makes use of the real geometry of the channel (single channel model), the other one considers the receiver to be “porous continuum”, which described with homogenized properties such as permeability and effective heat conductivity. The experimental parameters such as average solar heat flux and mass flow were taken into account in the models as boundary conditions. Various parameters such as the average air outlet temperatures, the temperature distributions and the solar-to-thermal efficiency were used for the comparison. The good correspondence between the experimental and numeric results of the both numeric investigations confirms the usefulness of the approach for further studies.

Keywords: Volumetric solar receiver; volumetric heat transfer coefficient; solar tower technology

1. Introduction

The rising interest in solar energy and its applications has led to an increasing research activity in this area. It belongs to two scientific areas: application of solar energy and new material’s properties investigation. The present paper belongs to second one.

The volumetric solar receiver as one of the main components of the system absorbs concentrated radiation and transfers heat to an air circuit, which feeds the boiler of a steam turbine. It has been used in solar energy since about 1985 and has been object of numerous investigations since then [1-4]. The material investigated is an improved Silicon Carbide honeycomb structure based on the state-of-the-art-technology shown in Fig. 1 (left), which has also been applied in the solar tower in Jülich [5]. It has been manufactured by St. Gobain IndustrieKeramik Rödenthal. The photo of the solar tower power station and the volumetric solar receivers are presented in Figure 1.

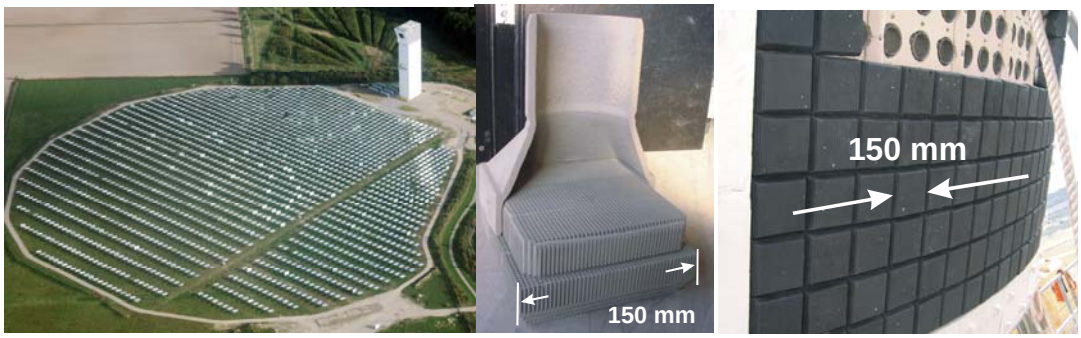

Fig. 1: Photographs of the Jülich Solar Tower, a part of the single absorber module and the solar receiver during installation

According to the short description of the volumetric solar receivers mentioned above the present research work has been undertaken in the network of the project "OVABSOL". It has been divided into two parts: experimental and numeric. The numerical part has been started to mainly develop tools, which can be used to

assess possible geometrical modifications, which are considered to improve the overall efficiency performance of the receiver system. So the aims of the study can be comprised as follows:
1. The determination of the influence of the geometrical variations on the efficiency and the maximum material temperature;
2. The determination of possible locations of the receiver's overheating;
3. The demonstration of the correspondence between experimental and calculated results.

2. Methodology

2.1 Experiment and experimental set-up

The volumetric solar receiver, which now is adapted on the new solar tower power station in Juelich (Germany), was used for study. The front view of the experimental set-up is shown in Fig. 2. It has been designed as an isolated tube, which is made of high temperature steel, equipped with a mass flow and several temperature sensors to measure the total heat gain of the air flow through the 140*140 mm volumetric solar receiver, which has to be mounted in the square opening of the test-bed.

Fig. 2: Experimental set-up for absorber testing (left) and set-up during the operation (right)

The set-up itself was located in the focus of the Xenon-High-Flux Solar Simulator. Typical radiation intensities of 400 – 600 kW/m² have been generated to have conditions close to the situation during an application in the solar tower. In order to avoid heat losses between the cylinder of the device and the sample the isolation material was used.

The thermal degree of efficiency was calculated according

$$\eta = \frac{Q_{Abs.\exp.}}{Q_{Radiation}} \tag{1}$$

Here, $Q_{Radiation}$ is the irradiative power from the lamps, $Q_{Abs.\exp.}$ is the measured heat content in the air:

$$Q_{Abs.\exp.} = \dot{M}_{inlet} \cdot c_P \cdot \left(T_{outlet} - T_{inlet}\right) \tag{2}$$

2.2 Numerical models

The numerical work can roughly be divided into two parts since two different models of the volumetric solar receiver have been developed. Both models are 3D-models and calculate the mass and thermal flows through the receiver module. They have been developed with the COMSOL Multiphysics code. The first one calculates the flow inside the real geometry of the absorber. Since this method requires a high number of elements in the flow region, it may be applied only to a small excerpt of the total volume of the receiver element. It is called the *single-channel-model*. The second model considers the volume of the receiver as a porous continuum with homogenized properties, which have been either experimentally determined (permeability, effective heat conductivity) or have been derived from the single-channel-model. It is called the *continuum model.*

For the *single channel model* the following COMSOL modules were used: (1) weakly compressible Navier-Stokes, (2) convection and heat conduction in the air and (3) heat conduction in the solid body. In case of the *continuum model* the Brinkmann-equation for porous materials has been used additionally to module (2) and (3) and instead of module (1) to describe the flow inside the receiver.

These models made it possible to find the velocity and temperature fields in the single channel and in the volume of the solar receiver. Using two heat transfer modules for the description of the heat transfer in the porous continuum – one for the air and one for the solid phase - gives the possibility of calculating two

temperatures. Energy exchange between these two modules is regarded be integrating a term describing the volumetric solid-to-fluid heat transfer. Because of the full symmetry of the geometry in the single channel as well in the whole receiver module, in both models only one quarter of the volume was calculated.

2.2.1 Boundary and area conditions of the numerical models

The concept of a volumetric heat source of the absorbed heat in the solar receiver was used for the calculation. As it is known from previous investigations the intensity of the radiation is attenuated in the cellular material due to a multiple reflection/absorption process, it can be described by an exponential law [2]:

$$I = I_0 \cdot e^{-\xi \cdot z} \tag{3}$$

Here, I_0 [W/m²] is the inlet heat flux value, ξ [1/m] is the extinction coefficient and z is the coordinate in flow direction. The heat flux I_0 used for the simulation was according to the average experimental value.

The extinction coefficient was found experimentally (through the transmittance measurements of the samples with different thickness) as it was described in [2]. The main area- and boundary conditions of the continuum model are presented below in Table 1 as a simplified specification. A more detailed description of this model is presented in [1].

Module	**Area conditions**	**Boundary conditions**	
		Inlet	**Outlet**
Weakly compressible Navier - Stockes	$\eta \cdot \nabla \left(\nabla u + (\nabla u)^T\right) = \rho \cdot u \cdot \nabla u$ - in air $\left(\frac{1}{\varepsilon_p}\right)\eta \cdot \nabla\left(\nabla u + (\nabla u)^T\right) = \left(\frac{\eta}{K}\right) \cdot u$ -in porous body	Velocity $u = u_0$	Pressure without the viscose stress $p = p_0$
Convection and Heat Conduction in air	$\nabla\left(-k \cdot \nabla T + \rho \cdot c_p \cdot u \cdot T\right) = q_0$ $q_0 = \alpha_{AV} \cdot (T_2 - T)$; $\alpha_{AV} = \alpha \cdot A_V = \frac{q}{T_w - T_L} \cdot A_V$	Temperature $T = T_0$	Convection flow $n \cdot (-k \cdot \nabla T) = 0$
Heat conduction in the solid body	$-\nabla\left(k \cdot \nabla T_2\right) = q_0$ $q_0 = I_0 \cdot \varepsilon_P \cdot \xi \cdot \exp(-\xi \cdot z) \cdot \cos\alpha + \alpha_{AV} \cdot (T - T_2)$ $\lambda_{por} = (1 - \varepsilon_P) \cdot 280{,}7 \cdot \exp(-0{,}0021 \cdot T2)$	Heat flow (Radiation) $n \cdot (k \cdot \nabla T_2) = q_0 + C \cdot \left(T_{amb}^4 - T_2^4\right)$ $q_0 = I_0 \cdot \cos\varphi \cdot (1 - \varepsilon_P) - (1 - \varepsilon_P) \cdot F \cdot (T_2 - T_0)$ $C = \varepsilon \cdot 5{,}67 \cdot 10^{-8}$	Temperature $T_2 = T$

Table 1. Area and boundary conditions of the continuum model

For the single channel model this specification looks simpler because the absorbed heat was regarded as a volumetric heat source in the wall of the solar receiver and by the inlet radiation heat flow on the inlet surface of the receiver. The area condition for the heat conduction module was determined in this model as

$$q_0 = Q_{absorb.} \cdot \frac{\xi \cdot \exp(-\xi \cdot z)}{A_Q} \tag{4}$$

Here A_Q is the surface of the wall cross-section, $Q_{absorb.}$ is the heat, which was absorbed by the receiver's wall. The inlet value of the radiation flux with the extinction coefficient and volumetric heat transfer coefficient were used for the determination of the volumetric heat source for the air and for the solid body. The volumetric heat transfer coefficient $\alpha \cdot A_V$ was calculated from the specific surface A_V [m²/m³] of the sample and the coefficient heat transfer, which was determined from the numeric heat flow distribution of the single channel model.

3. Results and Discussions

The single channel model was used to compare two different channel/wall geometries of the receiver element. Both geometries have been also investigated experimentally. A geometry modification of the whole

receiver module was investigated with the continuum model. The difference can be seen in Fig. 8. An additional frustum-like geometry has been chosen to homogenize the receiver front temperature. Also these two geometry versions have been additionally investigated experimentally.

3.1 The results of the single channel model

The two different channel/wall dimensions considered are shown in Table 2 together with the corresponding values of the specific surface area and additional flow and radiation parameters. Fig. 3 shows a schematic cross-sectional view of the two geometries considered.

Sample	**Channel width [m]**	**Wall thickness [m]**	**Specific surface of the sample [m²/m³]**	**Mass flow for the whole sample [kg/s]**	T_{inlet} **[°C]**	**Absorbed solar irradiative power in the considered unit cell** $Q_{absorb.}$ **[W]**
1	0.00218	0.00055	1170	$2.4 \cdot 10^{-3}$	45.1	1.16
2	0.00143	0.00025	2027	$2.5 \cdot 10^{-3}$	47.0	0.43

Table 2. Sizes and inlet parameters of the cylindrical samples

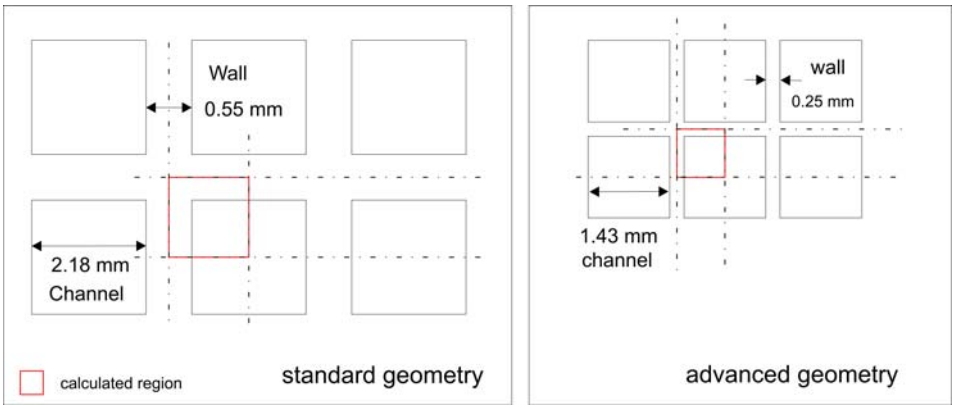

Fig. 3. Cross section of the cylindrical samples

This numeric model allows obtaining the results of velocity and temperature fields with the all thermo–hydraulic values of the investigated samples. As a first result, Figures 4 and 5 show the air temperature field in the channel and the heat flow distribution along of the channel depth correspondingly.

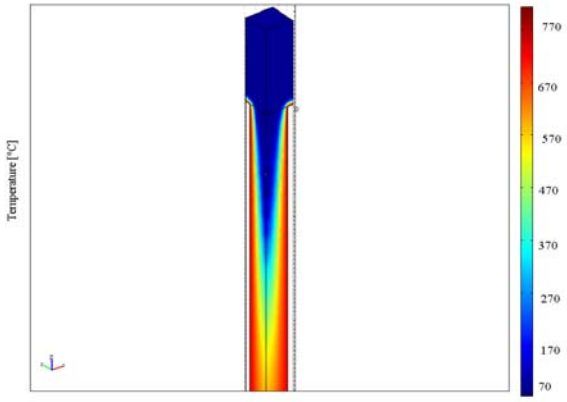

Fig. 4. Air temperature field in the channel

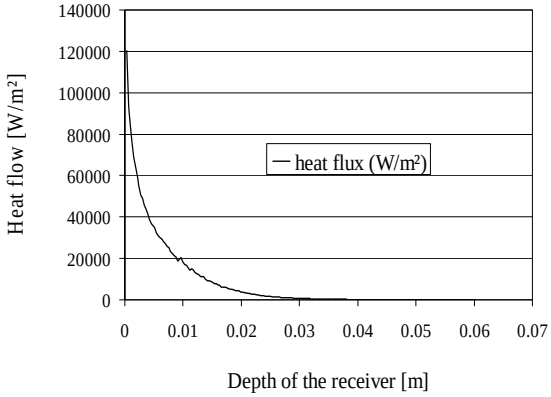

Fig. 5. Heat flow distribution in the channel

The air temperature field shows the expected large temperature gradients in the inlet area, which nearly approach zero after approximately 20 mm. These results are confirmed by the heat flow distribution, which was also used for the determination of the volumetric heat transfer coefficient.

Fig. 6 shows a comparison of the air and wall temperature distributions of the two samples. Because of the larger hydraulic resistance of sample 1, the hydrodynamic and thermal inlet path for this sample is longer than for the sample 2. For the sample 1 the inlet path is twice larger than for sample 2 (30 about 15mm). Additionally sample 2 shows a lower front temperature due to the increased surface area for heat transfer and the corresponding lower convective heat resistance. The comparison with the experimental data is shown in Table 3.

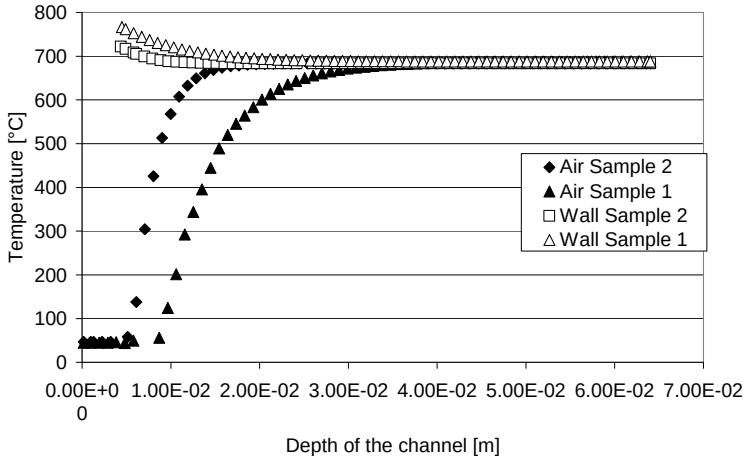

Fig. 6. Numeric temperature fields in the middle of the single channel

	Measured values		Simulated values	
	$\overline{T}_{out}$ [°C]	Thermal efficiency [%]	$\overline{T}_{out}$ [°C]	Thermal efficiency [%]
Sample 1	699	72	684	74
Sample 2	701	75	688	76

Table 3. Comparison of the outlet numeric and measured values

The average difference between the simulated and measured outlet temperatures and thermal efficiency is approximately 1-2%.

3.2. The results of the continuum model

The two receiver samples with and without the frustum were investigated experimentally as well as numerically with the continuum model. The irradiative flow in the experiment was non-homogeneous. It ranged from 300kW/m² to 700kW/m². In contrast to this a homogeneous flow, which was equivalent to the average experimental flow was assumed in the numerical model. This has become necessary due to limitations of the hardware capacity. The results with the measured inlet values were used for the data validation of the samples with and without the frustum.

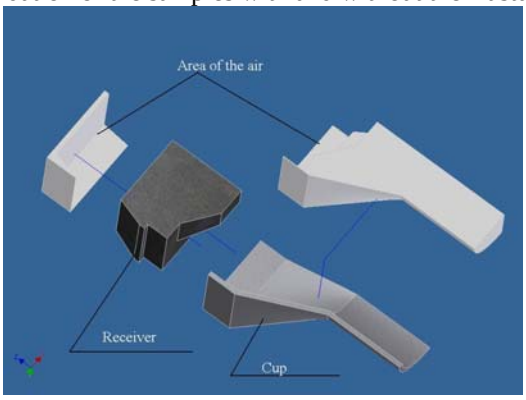

Fig. 7. The geometry of the continuum model

The receiver's real geometry with the "cup" was implemented in the simulation software. Figure 7 demonstrates this drawing with the frustum. The areas with only fluid flow are shown as white areas. Since the focus was put on the performance of the absorber material, heat transfer in the "cup wall" was not regarded to further reduce the model. Fig. 8 shows the velocity distributions as a comparison between the geometry with and without frustum. The velocity field has a more pronounced parabolic profile for the sample with frustum.

This velocity field leads to a larger velocity gradient in the cup volume because of the larger hydraulic resistance of this sample.

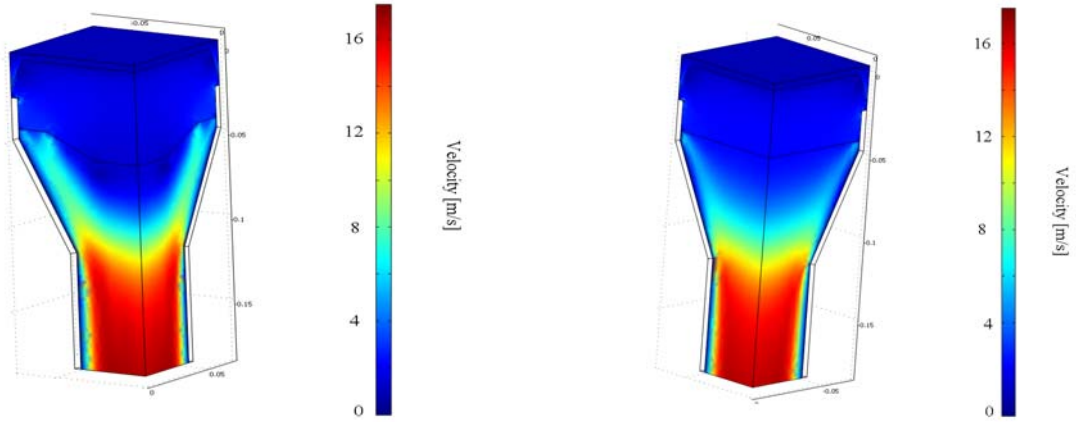

Fig. 8. Velocity fields in the two receiver geometries calculated with the continuum model

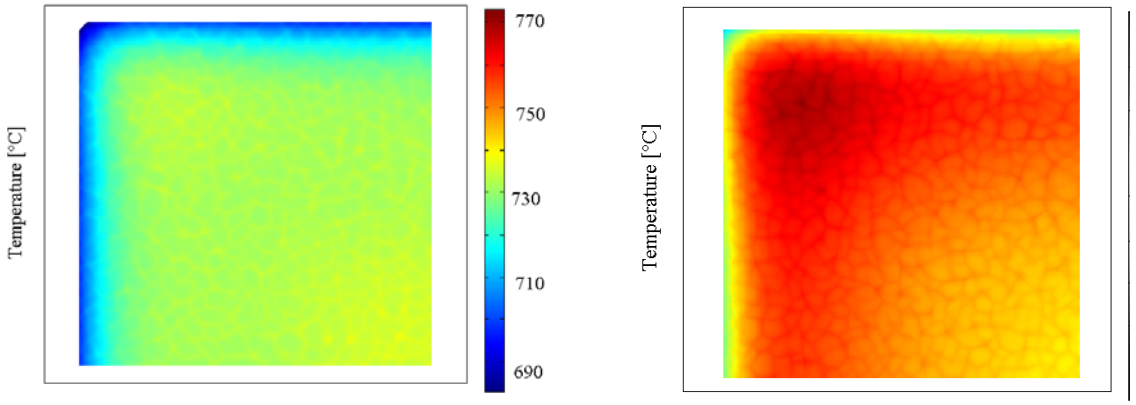

Fig. 9. Temperature of the receiver at the inlet with (with frustum left, without frustum right)

Fig. 9 shows the temperature fields at the inlet surfaces of the receiver with and without the frustum. The distribution is homogeneous for the sample with the frustum and significantly non-homogeneous for the sample without frustum. The inhomogeneous distribution can be explained by frictional effects at the edges of the receiver element close to the cup walls, which causes lower fluid velocities. The diagram in Fig. 10 shows the numeric temperature field both for the solid body and for the air in the volume of the volumetric solar receiver.

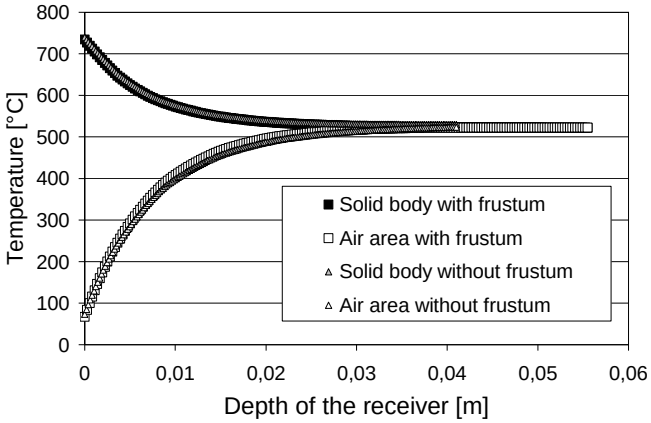

Fig. 10. The numerically determined temperature distribution in the center of the receiver volume in flow direction

The derived curves correspond to the temperature distributions in the middle of the receiver. The comparison of these values shows similar temperatures. After 30mm from the inlet in flow direction the difference between the temperatures of the solid body and air for the sample without frustum reaches 6 - 10°C and for

the sample with the frustum it vanishes. This shows the increased efficiency of the sample with the frustum, which also shows a slightly larger outlet air temperature.

	Inlet mass flow [kg/s]	$\overline{T}_{in.}$ [°C]	Experimental values		Numeric values	
			$\overline{T}_{out}$ [°C]	$\eta_{\exp.}$ [%]	$\overline{T}_{out}$ [°C]	η [%]
Sample 1	0.02	67	500,5	89,3	517	91,7
Sample 2	0.0189	74	500	82,3	538	89,1

Table 4. Comparison between the experimental and numeric results of the continuum model

Table 4 gives an overview of the main experimental and numerical results. Here, sample 1 is the one with frustum and sample 2 the one without frustum. The influence of the frustum on the efficiency is positive. The correspondence between experimentally and numerically determined air outlet temperature values is good.

4. Conclusion

The comparison of the numerical and experimental results shows a good correspondence for the single channel model with only 1–2% of divergence. The sample with the finer structure exhibits some advantages because of the smaller conductive and convective thermo resistance and the increased heat transfer surface. The numerical model predicts possible overheating regions of the receiver in the centre of the inlet surface and at the cylindrical surface of the cup in the outlet region.

The comparison between the geometry with and without frustum shows a larger thermal efficiency for the sample with frustum. This is true for both, the numerical as well as the experimental data.

Both of the presented models can be taken to predict temperatures and velocity distributions in the volumetric solar air receiver. The continuum model can be further improved if the measured inlet distribution of the radiation heat flow would be considered and the simulation mesh will be denser.

Acknowledgements

This study has been carried out in the framework of the project OVABSOL. It has been funded by the German Federal Ministry for the Environment. The support is greatfully acknowledged.

Nomenclature

u	velocity [m/s]
P	pressure [Pa]
η	dynamical viscosity [kg/m s]
ρ	density [kg/m³]
ε_p	porosity [-]
K	permeability [m²]
k	thermal conductivity [W/m K]
c_p	specific isobaric heat [J/kg K]
Q	heating power per unit volume for the convection heat transfer [W/m³]
α	convective heat transfer coefficient [W/m²K]
T	air temperature [K]
T_2	solid temperature [K]
A	inlet surface of the receiver [m²]
A_V	specific surface [m²/m³]
Re	Reynolds number [-]
$N\bar{u}$	Nusselt number [-]
q_0	heating power per unit volume for the conductivity heat transfer [W/m³]
m	mass flow [kg/s]
k_{por}	effective heat conductivity of the porous material [W/m K]
I_0	entrance heat radiation per unit surface [W/m²]
ξ	extinction coefficient of the radiation [1/m]
φ	Inlet angel of the radiation flow [°]
ε	Emissivity [-]
γ	Reflectivity [-]
z	coordinate along the main flow direction [m]

References:

[1] O. Smirnova, Th. Fend, P. Schwarzbözl, D. Schöllgen: Homogeneous and Inhomogeneous model for flow and heat transfer in porous materials as high temperature solar air receivers, Material of the conference COMSOL 2010

[2] Th. Fend, B. Hoffschmidt, R. Pitz–Paal, O. Reutter: Chapter: "Cellular ceramics use in solar radiation conversion", from the book M.Scheffler and P.Colombo: "Cellular ceramics: structure, manufacturing and applications", Willey – VCH GmbH & Co. KgA, Weinheim, 2005

[3] B. Hoffschmidt: „Comparison and evaluation of different concepts of volumetric radiation receivers“, Doctoral Thesis RWTH Aachen, DLR– Forschungsbericht 97-35, (1997), p.38 - 41

[4] M. Becker, Th. Fend, B. Hoffschmidt, R. Pitz–Paal: Theoretical and numerical investigation of flow stability in porous materials applied as volumetric solar receivers, 1 Solar Energy 80 (2006) p.1241 - 1248

[5] Th. Fend, B. Hoffschmidt, R. Pitz–Paal, O. Reutter, P. Rietbrock: Porous materials as open volumetric solar receivers experimental determination of thermophysical and heat transfer properties, Energy 29 (2004), (5-6), p.823 - 833